Available online at www.sciencedirect.com
SCIENCE DIRECT
Aerosol Science 37 (2006) 386–401
Journal of Aerosol Science
www.elsevier.com/locate/jaerosci

Soot aggregates, superaggregates and gel-like networks in laminar diffusion flames

Wongyo Kim, Christopher M. Sorensen*, Danny Fry, Amitabha Chakrabarti

Department of Physics, Kansas State University, Manhattan, KS 66506-2601, USA

Received 23 September 2004; received in revised form 3 May 2005; accepted 16 May 2005

Dedicated toThis paper is dedicated to Professor Dan Rosner on the occasion of his seventieth birthday.

Abstract

We show that soot formed in laminar diffusion flames of heavily sooting fuels evolves through four distinct growth stages which give rise to four distinct aggregate fractal morphologies. Each successive stage grows upon the previous stage; hence aggregates of one morphology, parameterized by a fractal dimension, form larger superaggregates or gels of a different morphology with a different fractal dimension. These results were inferred from large and small angle static light scattering from the flames, microphotography of the flames, and analysis of soot sampled from the flames. These results and the analysis were substantiated by comparison to computer simulations. The growth stages occur approximately over four successive orders of magnitude in aggregate size. Each growth stage is a fundamental physical process: Stages 1 and 3 are diffusion limited cluster aggregation in three and two dimensions, respectively; Stages 2 and 4 are percolation in three and two dimension, respectively.

Keywords: Flames; Combustion; Fractal aggregates; Superaggregates; Gelation

1. Introduction

Soot is a product of combustion, our primary source of energy. Luminous soot in a flame enables radiative coupling to the environment. Smoke, soot released from a flame, kills in accidental fires, and detection of smoke is a primary step in fire safety. Often undesirable, it is the dominant particulate pollutant

* Corresponding author. Tel.: +1 7855321626; fax: +1 7855326806.
E-mail address: sor@phys.ksu.edu (C.M. Sorensen).

0021-8502/$ - see front matter © 2005 Elsevier Ltd. All rights reserved.
doi:10.1016/j.jaerosci.2005.05.022

Table 1
The realm of supersoot

Growth process	Stage 1	Stage 2	Stage 3	Stage 4
	3d DLCA	3d percolation or restructuring	2d DLCA	2d percolation
Fractal dimension	1.8	$\simeq 2.6$	1.4	$\simeq 1.9$
Morphology	Aggregates	Superaggregates	Supersuperaggregates	2d gel network
Crossover length scale	$\sim 1\,\mu m$		$\sim 10\,\mu m$	$\sim 100\,\mu m$

in the atmosphere, hence it has a major effect on our climate and our health. Key physical parameters for soot are its size and morphology which fundamentally govern all the situations above.

The current view of soot formation and growth in flames involves a series of steps including fuel thermal decomposition to small radicals (Palmer & Cullis, 1965; Glassman, 1988) that react to form polyaromatic hydrocarbons (D'Anna, D'Alesso, & Minutolo, 1994; Dobbins & Subramaniasivam, 1994; Dobbins, Fletcher, & Chang, 1998; Frenklach, 2002) that subsequently nucleate, coalesce and dehydrogenate to yield roughly spherical, graphitic, primary particles of soot with diameters in the few tens of nanometer range (Lahaye & Prado, 1981). After this, the physical process of three-dimensional diffusion limited cluster aggregation (DLCA) (Meakin, 1999; Oh & Sorensen, 1997) proceeds to make noncoalesced clusters which have a fractal morphology with a universal fractal dimension of $D \simeq 1.8$ (Samson, Mulholland, & Gentry, 1987; Dobbins & Megaridis, 1987; Zhang, Sorensen, Ramer, Olivier, & Merklin, 1988; Sorensen, Cai, & Lu, 1992; Koylu & Faeth, 1992). Thereafter environmental restructuring might occur, but with this single step of DLCA, the present description of in-flame soot growth ends.

Our work of the past few years has indicated that this picture is seriously incomplete for the soot produced in heavily sooting laminar diffusion flames. This includes the observation of gel-like networks of soot (Sorensen, Hageman, Rush, Huang, & Oh, 1998), flat, two-dimensional soot (Sorensen & Hageman, 2001), and soot with a fractal dimension of 2.6 that was found in a variety of different flames (Sorensen, Kim, Fry, Shi, & Chakrabarti, 2003; Kim, Sorensen, & Chakrabarti, 2004).

In this paper we build upon this previous work, report new data extending these observations to flames of other fuels, and describe a new, multi-stage growth scenario that coherently connects both our previous observation and the new ones reported here. We find that there can be four different and successive stages of soot growth in laminar diffusion flames of heavily sooting fuels. Each growth stage yields a unique soot cluster morphology over successive length scales. This successive nature leads to what we term a "superaggregate" morphology which is meant to imply that aggregates of a specific fractal dimension formed by a specific growth process come together by a different growth process to form a larger aggregate of a different fractal dimension; this is the superaggregate, an aggregate of aggregates. Moreover, these growth processes, of which there are four, and their concomitant morphologies are fundamental physical processes hence apply to all flames and indeed all particulate systems given the proper initial conditions.

We lead off with our final results in Table 1. We have chosen to begin with the end because we think that with the end in mind our reader will better understand the steps along the way. Table 1 shows four successive growth stages with their resulting morphologies. Length scales dividing the stages are also shown. Stage 1 is the well known diffusion limited cluster aggregation (DLCA) process that leads to fractal aggregates with a fractal dimension of $D \simeq 1.8$. Stage three is also a DLCA process, but one

confined to two dimensions. Stages 2 and 4 are percolation processes that occur when the DLCA clusters of Stages 1 and 3 become densely packed, in either three or two dimensions, respectively.

Our work is relevant to soot formation in common laminar diffusion flames in which the fuel and the oxidizer (e.g., oxygen in air) flow in a parallel manner in adjacent regions and diffuse together at the flame front. A candle is a typical example. Other more complex flames of technical importance, e.g., turbulent diffusion flames, still involve diffusion of fuel and oxidizer across a flame front; hence our work is likely relevant to these important flames as well. Finally, the transition from diffusion limited aggregation to percolation when the system becomes, "cluster dense" (see below) is very likely universal to all particulate systems, both colloidal and aerocolloidal, that gel.

2. Experimental methods

In our experiments static light scattering was used to measure the structure of the soot aggregates in the flames (Sorensen, 2001). These measurements gave the scattered intensity $I(q)$ as a function of q, the scattering wave vector, $q = 4\pi\lambda^{-1}\sin(\theta/2)$ where λ is the optical wavelength and θ is the scattering angle. An argon ion laser operating at $\lambda = 488\,\text{nm}$ was used as the light source. Both a small angle apparatus (Ferri, 1997), with $150\,\text{cm}^{-1} \leqslant q \leqslant 2.7 \times 10^4\,\text{cm}^{-1}$ (ca. $0.07° \leqslant \theta \leqslant 12°$) and a large angle apparatus, with $10^4\,\text{cm}^{-1} \leqslant q \leqslant 1.4 \times 10^5\,\text{cm}^{-1}$ (ca. $5 \leqslant \theta \leqslant 70°$) were used. A diagram of the apparatus is presented in Fig. 1. Since q^{-1} is the length scale of the scattering experiment, these apparatii allow us to probe soot morphologies from 70 nm to nearly 60 μm.

Direct observation of the very large soot in the flame and the flame structure was accomplished using a 10 power photomicroscope with an object distance of 15 cm. The flame was backlit by a 7 ns pulsed Nd:YAG laser with $\lambda = 532\,\text{nm}$ shining on a white background behind the flame.

Samples for transmission electron microscope (TEM) analysis were taken by thermophoretic deposition onto TEM grids inserted quickly and briefly into the flame as originally described by Dobbins and Megaridis (1987) and used previously in this laboratory (Cai, Lu, & Sorensen, 1993; Sorensen & Hageman, 2001).

The flames were all laminar diffusion flames in ambient air. Gaseous fuels at controllable flow rates emanated from a brass tube 0.9 cm inside diameter. Liquid fuels were burned with a simple wick burner with wick diameter of 0.6 cm. Solid naphthalene was molded into a candle 0.6 cm in diameter. The fuels used are listed in Table 2.

3. Results

3.1. Stages 1 and 2

Fig. 2a shows the scattered intensity as a function of the wavevector, $I(q)$, for an acetylene flame from previous work (Sorensen et al., 2003). Low in the flame, i.e., for heights above burner of $h < 2\,\text{cm}$, the scattering is isotropic for low q but then bends over to a power law with slope ca. -1.8. The bend occurs near $q \simeq 3 \times 10^4\,\text{cm}^{-1}$ to imply an aggregate size of $q^{-1} \simeq 0.3\,\mu\text{m}$. This corresponds to the often observed and well known phase of submicron, fractal dimension $D \simeq 1.8$ soot which is a result of a 3d DLCA aggregation process (Meakin, 1999; Oh & Sorensen, 1997) (stage 1, Table 1). With increasing

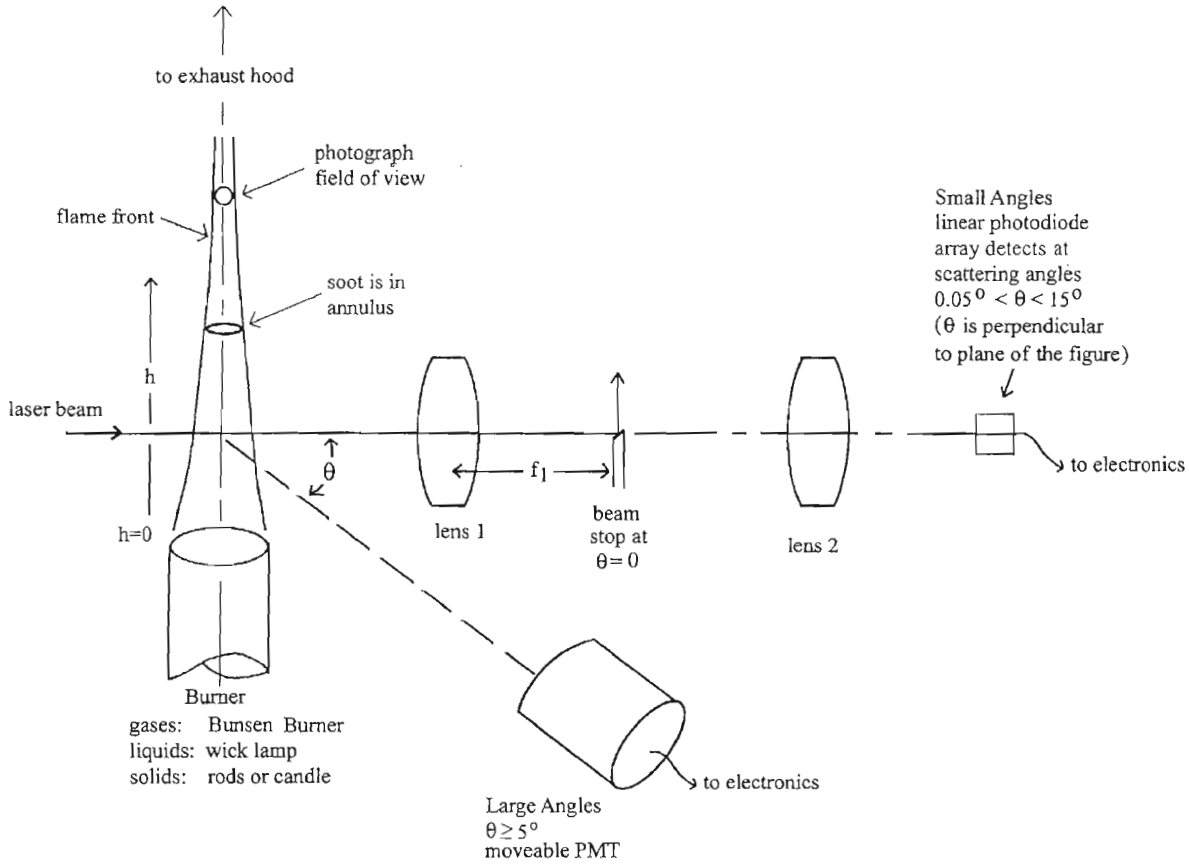

Fig. 1. Diagram of the experimental set-up.

height above burner, which corresponds to increasing time for the soot to grow, a very intense, second phase appears at low q. In the region ca. $800 \leqslant q \leqslant 8000\ \mathrm{cm}^{-1}$ the slope of the log–log plot indicates a power law $I(q) \sim q^{-2.6}$ for this second phase. Note that the $q^{-1.8}$ regime remains at large q. This scattering behavior may be interpreted to indicate a phase of ca. 12 μm soot with a fractal dimension of $D \simeq 2.6$ for length scales of 1.2 μm to 12 μm (stage 2) and $D \simeq 1.8$ for scales smaller than 0.3 μm down to the primary particle size (ca. 25 nm as determined by TEM). Results for the toluene (Fig. 3) and 1-methylnaphthalene (Fig. 4) flames, also from previous work (Kim et al., 2004) show the same behavior. We have shown (Kim et al., 2004) that this large, $D \simeq 2.6$ phase occurs in laminar diffusion flames of heavily sooting fuels as quantified by the thermal sooting index (TSI) as defined by Calcote and Manos (1983) and Olson, Pickens, and Gill (1985), specifically when $\mathrm{TSI} \geqslant 10 \pm 2$ (roughly, the larger the fuel TSI, the sootier the flame). Otherwise, for less sooty flames only the submicron, $D \simeq 1.8$ soot is seen; no $D \simeq 2.6$ phase nor the subsequent phases to be described below (see Table 2).

Table 2
Fuels, threshold soot indices (TSI), and measured fractal dimensions within the 4 stages of soot growth. Dash means no measurements were attempted although stage 1 is expected for all flames

Fuel	TSI	Stage 1	Stage 2	Stage 3	Stage 4
Gases					
Methane	~ 0	1.8	No	No	No
Ethylene	0.7	1.8	No	No	No
Acetylene	11	1.7	2.7	1.44	1.9
Liquids					
Hexadecane	5.8	–	No	No	No
Isooctane	6.4	–	No	No	No
1-Hexadecene	11	–	No	No	No
JP5 Fuel	–	–	Marginal	No	No
Decaline	15	–	Marginal	No	No
Toluene	44	1.7	2.6	1.39	1.9
Styrene	67	–	2.6	–	–
1-Methyl naphthalene	91	1.8	2.5	(1.4)	1.9
Solid					
Naphthalene	100	–	2.7	1.5	1.9

To corroborate the light scattering measurements soot was sampled from the flame using a well established thermophoretic technique (Dobbins & Megaridis, 1987). Fig. 2b (right side) shows an example of submicron soot (stage 1) collected low in the acetylene/air diffusion flame and Fig. 2b (left side) shows an example of supermicron soot superaggregates (stage 2) collected high in the flame. Visual inspection shows the much more compact appearance of the large soot than the small, qualitatively supporting a larger fractal dimension for the larger aggregate. Previous real space analysis of projected images of submicron soot have confirmed the $D \simeq 1.7$ to 1.8 fractal dimension (Dobbins & Megaridis, 1987; Koylu & Faeth, 1992; Cai et al., 1993).

For the large soot aggregates we applied an analysis developed by Jullien, Thouy, and Ehrburger-Dolle (1994) for 2d projected images of 3d fractal aggregates with $D > 2$. Using simulations they found the relation

$$D = 3 - (D_p - 1)^{2/3} \tag{1}$$

between the perimeter fractal dimension D_p and the true 3d mass fractal dimension D. Fig. 5 gives more examples of these large, relatively dense soot aggregates. We measured 10 large clusters to find $D_p = 1.26 \pm 0.06$. This D_p implies $D = 2.6 \pm 0.06$, in excellent agreement with our light scattering results. Furthermore, the average size we measure for the collected aggregates is $10 \pm 3\,\mu m$, also in excellent agreement with light scattering.

The mechanism that creates this second phase is still somewhat uncertain. One scenario is that it represents 3d DLCA clusters with initial $D \simeq 1.8$ that have grown to ca. 10 μm or larger and then restructured to a denser $D \simeq 2.6$ (hence smaller) under the shear stress at the flame front. There is evidence for shear restructuring of DLCA aggregates to larger fractal dimensions in colloids (Martin, Wilcoxon, Schaefer, & Odinek, 1990; Carpineti, Ferri, & Giglio, 1990; Jung, Amal, & Raper, 1996; Selomulya, Bushell, Amal, & Waite, 2002). There is, however, no evidence for ca. 10 μm, $D \simeq 1.8$

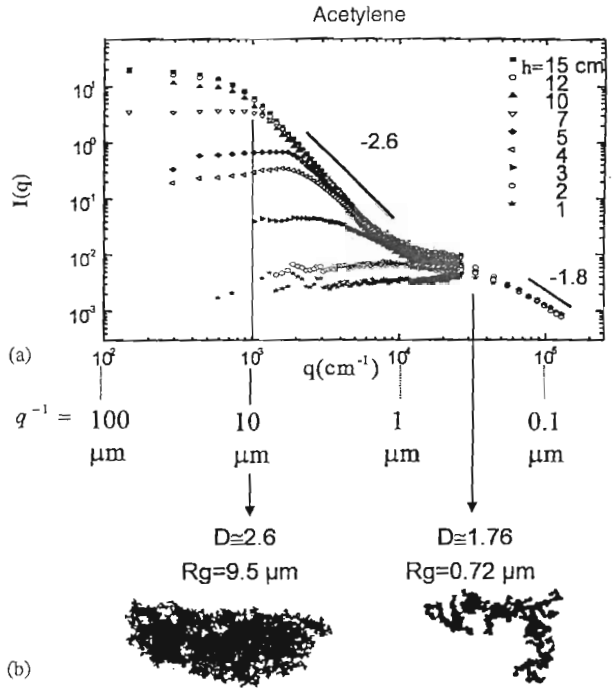

Fig. 2. (a) Static light scattered intensity as a function of scattering wavevector from an acetylene/air flame at various heights above burner h. Inverse q values represent length scales. (b) On left is soot superaggregate with fractal dimension $D \simeq 2.6$ and radius of gyration $R_g = 9.5\,\mu m$ collected from the flame at $h = 12\,cm$. On the right is soot aggregate with $D \simeq 1.76$ and $R_g = 0.72\,\mu m$ collected from the flame at $h = 2\,cm$. Arrows from (a) to (b) indicate correspondence between the aggregates and the scattered light spectra.

aggregates in our flames necessary for restructuring. A second scenario, that we consider more likely and have described previously (Sorensen et al., 2003; Kim et al., 2004), involves a percolation process that occurs when the DLCA aggregates become "cluster dense." During any aggregation process both the mean cluster size and the mean nearest neighbor separation increase with time. If particles come together and coalesce to form compact aggregates, the ratio of mean separation to size will remain constant. However, noncoalescing particles yield noncompact, often fractal, aggregates with a fractal dimension less than the spatial dimension. Then with growth the mean separation to size ratio will decrease. This will yield a situation in which the clusters begin to fill all space, a situation we call "cluster dense." Our computer simulations have demonstrated this and shown that the cluster dilute (i.e., mean separation to size ratio large) DLCA growth crosses over to a percolation process in which the dense clusters jam together (Fry, Chakrabarti, Kim, & Sorensen, 2004). The result is a percolated, $D \simeq 2.6$ *superaggregate* of the smaller $D \simeq 1.8$, DLCA aggregates. Structure factors of our simulations, Fig. 6 is an example, show both the $D \simeq 2.6$ and $D \simeq 1.8$ regimes as seen in our flame data, e.g., Figs. 2a, 3 and 4. We have shown that the crossover length scale between the $D \simeq 1.8$ and 2.6 regimes is consistent with soot volume fraction measurements (Sorensen et al., 2003; Fry et al., 2004; Fry, Sintes, Chakrabarti, & Sorensen, 2002). Fig. 7 shows a diagram of our vision of a superaggregate.

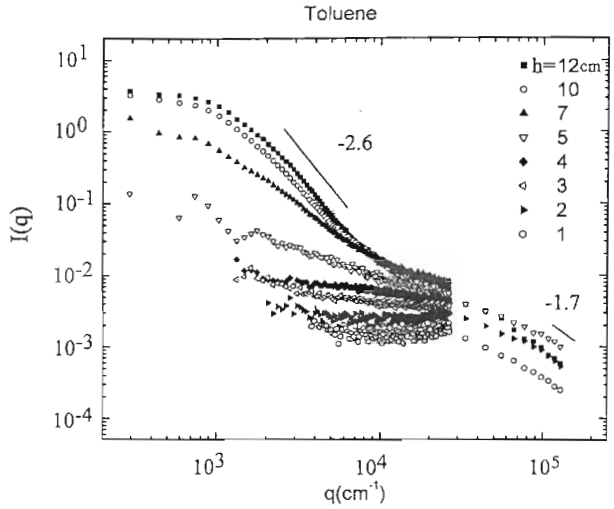

Fig. 3. Static light scattered intensity as a function of scattering wavevector from a toluene/air flame at various heights above burner h.

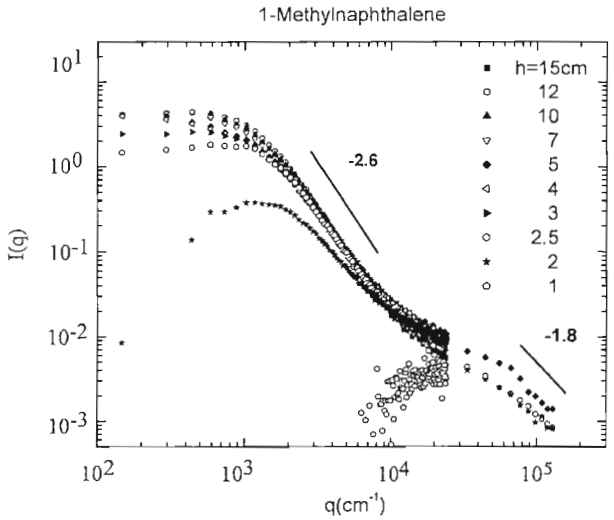

Fig. 4. Static light scattered intensity as a function of scattering wavevector from a 1-methylnaphthalene/air flame at various heights above burner h.

3.2. *Stage 3*

Figs. 8a, 9a, and 10a show 7 ns exposure photographs of submillimeter soot in acetylene, toluene and naphthalene flames, respectively. These clusters are flat, quasi-2d (they are seen face on in Figs. 8a, 9, and 10a) similar to those seen previously in acetylene flames (Sorensen & Hageman, 2001). Following

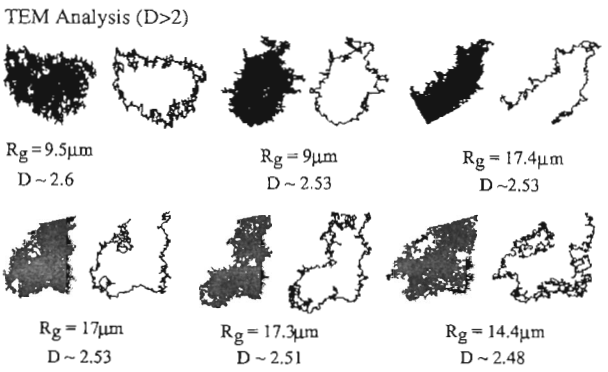

Fig. 5. Transmission electron micrographs of large soot (supersoot) aggregates collected from an acetylene/air flame at a height above burner of $h = 12$ cm. Next to each image is the perimeter of the aggregate. In many cases the perimeter is incomplete due to partial occultation by the grid wires of the TEM grid. Values for the radius of gyration R_g and mass fractal dimension D are given for each cluster. D was determined from the perimeter fractal dimension D_p via. Eq. (1).

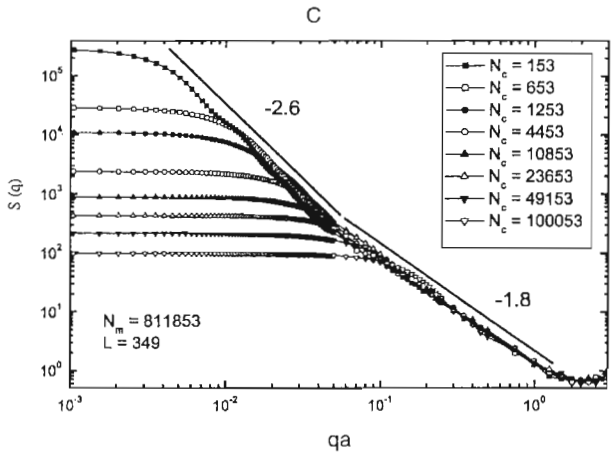

Fig. 6. Structure factor of an off-lattice, DLCA simulation in a cubic box (3d) of side L (measured in primary particle radii a) with N_m primary particles. The structure factor $S(q)$ is proportional to the light scattered intensity $I(q)$ for a real system. $S(q)$ evolves with increasing time, as represented by the decreasing number of clusters, N_c, from a system with solely 3d, DLCA, $D \simeq 1.8$ aggregates to a system with percolated superaggregates with $D \simeq 2.6$ composed of the smaller $D \simeq 1.8$ aggregates.

that previous analysis, cluster images were digitized into binary format (Figs. 8b, 9b, and 10b) then were analyzed to determine the number of dark pixels N_p, which is proportional to cluster mass, and R_g, the cluster radius of gyration for each cluster. If the clusters are fractal, then the well known relationship

$$N_p \sim R_g^D \tag{2}$$

will hold. Eq. (2) implies that when N_p vs. R_g is plotted for many clusters on a log–log graph, linearity indicates fractal morphology, and the slope yields the fractal dimension. Figs. 8c, 9c, and 10c show such plots for these three flames with fractal dimensions of $D = 1.44 \pm 0.05$, 1.39 ± 0.05 and 1.50 ± 0.06,

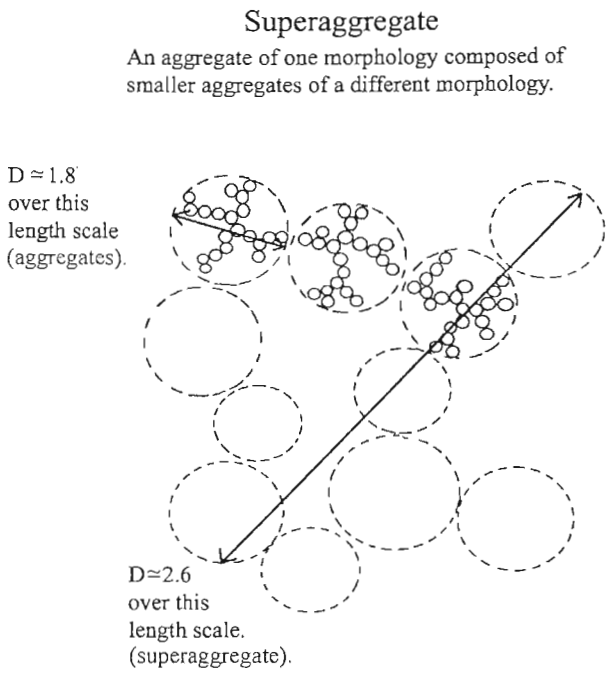

Fig. 7. Diagram of a superaggregate.

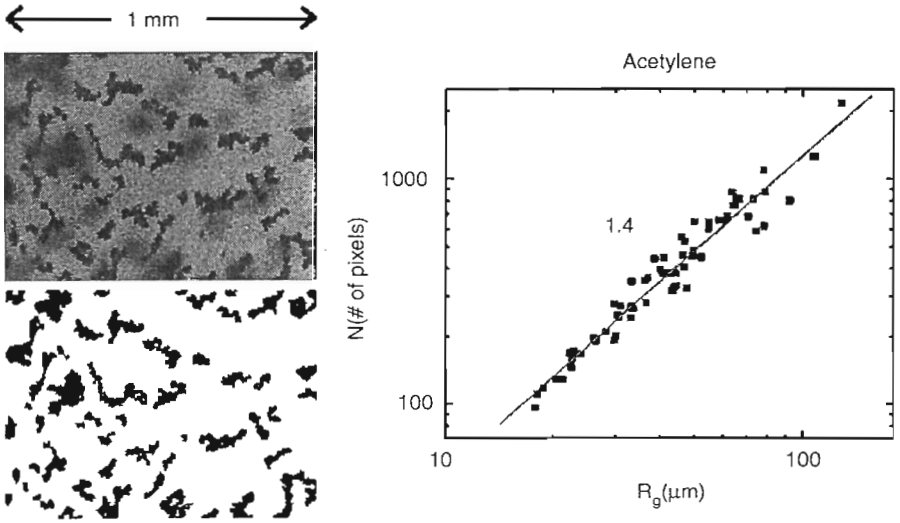

Fig. 8. (a) 7 ns exposure photograph of soot in an acetylene/air flame at a height above burner of $h = 10$ cm. The width of the picture is 1 mm. (b) Binary digitized version of (a). (c) Number of pixels per aggregate versus radius of gyration for an ensemble of soot clusters including those in (a).

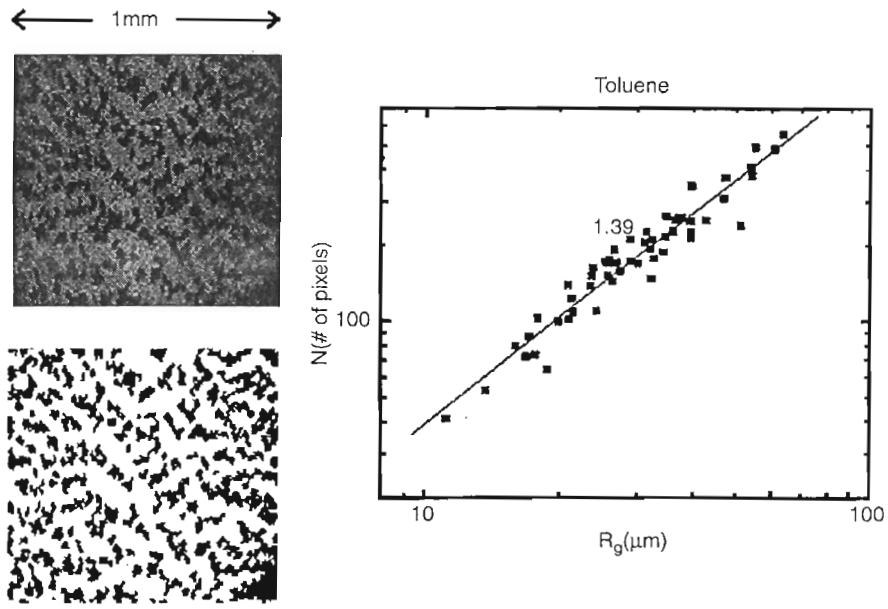

Fig. 9. (a) 7 ns exposure photograph of soot in a toluene/air flame at a height above burner of $h = 10$ cm. The width of the picture is 1 mm. (b) Binary digitized version of (a). (c) Number of pixels per aggregate versus radius of gyration for an ensemble of soot clusters including those in (a).

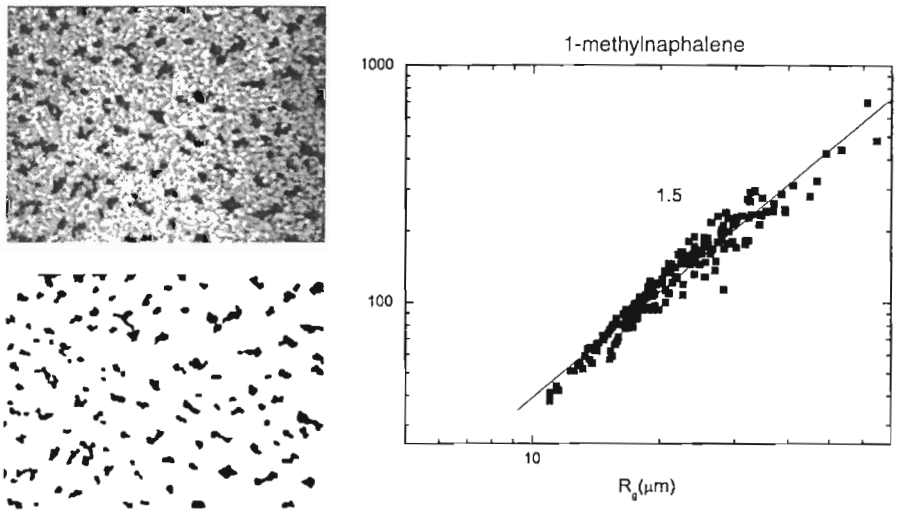

Fig. 10. (a) 7 ns exposure photograph of soot in a naphthalene/air flame at a height above burner of $h = 10$ cm. The width of the picture is 1 mm. (b) Binary digitized version of (a). (c) Number of pixels per aggregate versus radius of gyration for an ensemble of soot clusters including those in (a).

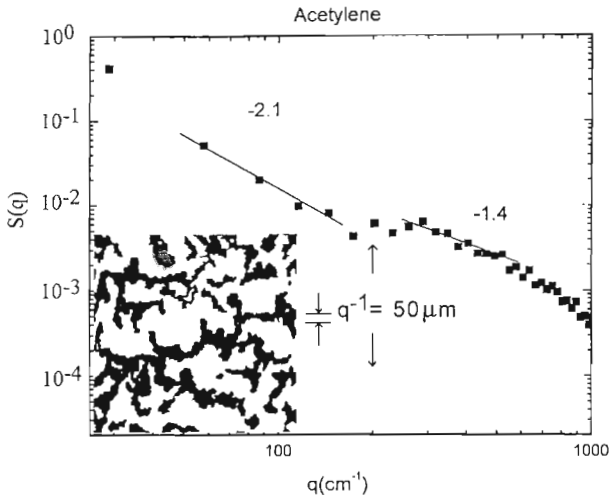

Fig. 11. Fourier transform, hence structure factor $S(q)$, of the digitized image of a flame soot network, lower right corner, in a laminar acetylene/air diffusion flame at a height above burner of $h = 12$ cm. The crossover between power laws as indicated by the up arrow has a value of about $q = 200\,\text{cm}^{-1}$, down arrow. This corresponds to a length scale of $q^{-1} = 50\,\mu\text{m}$ which is indicated by the scale indicator to the right of the digitized image.

respectively. These values are included in Table 2. Thus all three flames yield flat aggregates with a fractal dimension of ca. 1.45 over length scales of ca. 10 to 100 μm. This morphology is stage 3 in Table 1. Similar results were found previously (Sorensen & Hageman, 2001) (and reproduced in this study) for acetylene.

Sorensen and Hageman (2001), concluded that this phase of soot occurs because the soot, which is confined to an annular flame front, becomes larger than the thickness of the flame front and thus is confined in an effectively two-dimensional (2d) space in which to aggregate. Simulations of 2d DLCA yield fractal aggregates with $D = 1.44$ consistent with our measurements (Meakin, 1999). Thus we named this phase "two-dimensional soot." Since this phase of soot is immediately larger than the second phase of soot described above, and since it has a different fractal dimension, 1.45 as opposed to 2.6, we propose that it is a third phase of soot consisting of 2d, DLCA aggregates of the superaggregates of phase two. We call these aggregates of superaggregates "supersuperaggregates." They have three levels of structure, each level having its own fractal dimension, and two crossover length scales, one between each consecutive level, as outlined in Table 1, stages 1, 2, and 3.

3.3. Stage 4

Flame spanning networks of soot are seen higher in the flames or at larger fuel flow rates. Examples of digitized images for four flames, acetylene, toluene, 1-methylnapthalene, and naphthalene, are given in the lower right hand corners of Figs. 11–14, respectively. Once again we stress that as for the supersuperaggregates these networks are confined to the thin cylindrical annulus of the flame front. In previous work we argued that this network was a gel because its ramified structure spanned the available space (Sorensen et al., 1998). We will now support that argument quantitatively. Once again we photographed

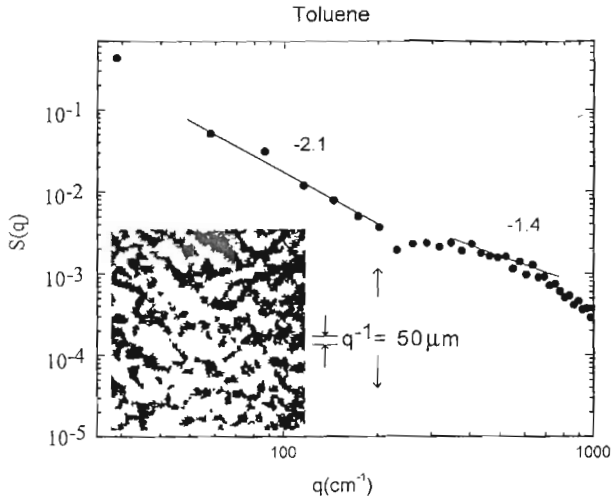

Fig. 12. Fourier transform, hence structure factor $S(q)$, of the digitized image of a flame soot network, lower left corner, in a laminar toluene/air diffusion flame at a height above burner of $h = 12$ cm. The crossover between power laws as indicated by the up arrow has a value of about $q = 200\,\mathrm{cm}^{-1}$, down arrow. This corresponds to a length scale of $q^{-1} = 50\,\mu\mathrm{m}$ which is indicated by the scale indicator to the right of the digitized image.

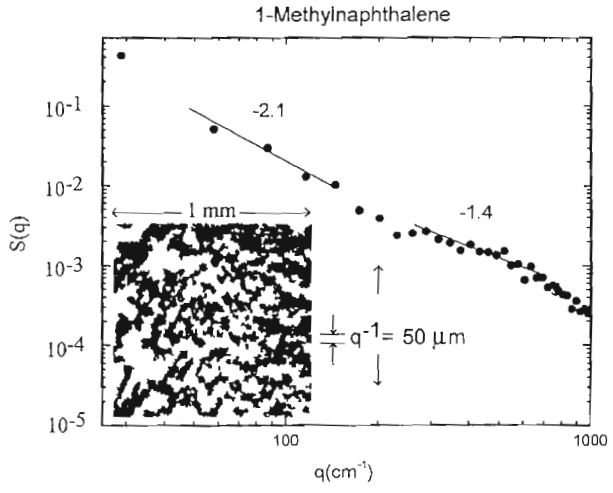

Fig. 13. Fourier transform, hence structure factor $S(q)$, of the digitized image of a flame soot network, lower left corner, in a laminar 1-methylnaphthalene/air diffusion flame at a height above burner of $h = 12$ cm. The crossover between power laws as indicated by the up arrow has a value of about $q = 200\,\mathrm{cm}^{-1}$, down arrow. This corresponds to a length scale of $q^{-1} = 50\,\mu\mathrm{m}$ which is indicated by the scale indicator to the right of the digitized image.

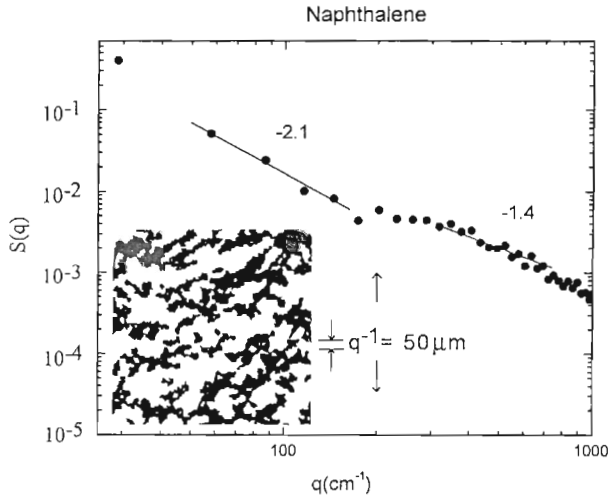

Fig. 14. Fourier transform, hence structure factor $S(q)$, of the digitized image of a flame soot network, lower left corner, in a laminar naphthalene/air diffusion flame at a height above burner of $h = 12$ cm. The crossover between power laws as indicated by the up arrow has a value of about $q = 200\,\mathrm{cm}^{-1}$, down arrow. This corresponds to a length scale of $q^{-1} = 50\,\mu\mathrm{m}$ which is indicated by the scale indicator to the right of the digitized image.

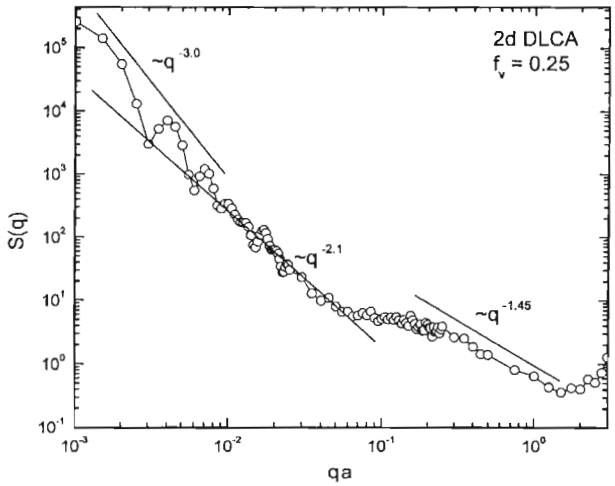

Fig. 15. Structure factor of an off-lattice, DLCA simulation on a square lattice (2d) of side $L = 1000\,a$, where a is the circular monomer radius. The $q^{-3.0}$ regime is the Porod regime of the square box with $q^{-(d+1)}$, $d = 2$ and interference ripples due to the sharp edges of the box. The $q^{-2.1}$ regime is due to percolated superaggregates with a fractal dimension of 1.9. The $q^{-1.45}$ regime is due to $2d$, DLCA aggregates that make up the superaggregate. The volume fraction of monomers is $f_v = 0.25$.

the flame with the photomicroscope and a 7 ns exposure. These pictures were cropped to observe only the central 60% to avoid the curvature of the flame front. This yielded pictures 1.0 mm^2. Analysis of the gel network structure was accomplished by Fourier transformation of the digitized images obtained with the photomicroscope. Analysis of Fourier transform data at low q is hampered by the finite size of the picture that is 1 mm^2. The raw data show "interference ripples" at low q due to the hard edges of the picture box. To remove this box effect the uniform box was Fourier transformed, and the raw data were normalized with this to yield a corrected structure factor showing only the structure of the image, not the picture box. The resulting q-space function is a structure factor, $S(q)$ vs. q, that is proportional to a light scattering result, $I(q)$. Results for the four different flames are given in Figs. 11–14.

In each analysis at large $q(>1000\,cm^{-1})$ a slope of -3 is found (not shown in the figures). We interpret this as Porod scattering, $I(q) \sim q^{-(d+1)}$ for $d = 2$, to imply that the 2d image is uniformly black for lengths $q^{-1} < 10^{-3}$ cm $= 10\,\mu m$. This value is consistent with our photographic resolution limit which we estimate to be 5 μm, i.e., for length scale less than 5 to 10 μm the image is uniformly black and two dimensional. This is a mild test of our analysis.

For $200 \leqslant q \leqslant 700\,cm^{-1}$, which corresponds to length scales q^{-1} of 14–50 μm, the $I(q)$ data roughly follow a power law of $I(q) \sim q^{-1.4}$. This is a poor resolution observation of a remnant of the 2d, $D \simeq 1.45$ supersuperaggregates, stage 3. We propose that it is these supersuperaggregates that come together to form the gel network.

In each of the Figs. 11–14 a crossover between power laws of $-1.4-2.1$ occurs in each structure factor at approximately $q = 200\,cm^{-1}$, as indicated in each figure. This corresponds to a length of $q^{-1} = 50\,\mu m$. This length is drawn to scale to the right of each digitized image. One can see that this roughly corresponds to the length scale where the figure crosses over from cluster to network length scales.

For $30 \lesssim q \lesssim 200\,cm^{-1}$, i.e., length scales of 50–300 μm, data for all flames showed a $I(q) \sim q^{-2.1}$ power law. This power law can be understood by comparing to simulations of 2d DLCA aggregation we performed. These simulations were allowed to proceed until the system percolated to form a gel network. Fig. 15 shows the structure factor for a simulation with nearly 4×10^5 monomers allowed to aggregate via Brownian motion in a 2d box until only one large cluster formed. Real space analysis of this large cluster showed it had a fractal dimension of 1.9, consistent with a 2d, percolation cluster (Stauffer & Aharony, 1992). The entire box was Fourier transformed for direct comparison to the flame network data. The results in Fig. 14 are strikingly similar to the flame data including both the $q^{-1.4}$ and $q^{-2.1}$ regimes (and interference ripples due to the finite system size). The power law exponent (2.1) does not equal the fractal dimension, $D \simeq 1.9$, in this case because D is almost equal to the spatial dimension d. Note that when $D = d$, a Porod law with power—$(d+1)$ results, which would be q^{-3} for this 2d situation. Thus the $q^{-2.1}$ power law implies that the fractal dimension of the network, in both the flame soot and the simulation, is less than but very close to the spatial dimension of $d = 2$. This strongly supports the contention that the gel-like network structure in our flames is the result of a 2d percolation of the $D \simeq 1.4$, 2d DLCA, supersuperaggregates.

4. Conclusions

Table 1 above summarizes our results and presents a new description of aggregate growth and concomitant morphologies of soot in laminar diffusion flames. There are four consecutive stages of growth: 3d DLCA, 3d percolation, 2d DLCA, and 2d percolation. Each pair of stages is separated by length scales of

approximately 1, 10 and 100 μm. Each process adds another layer of structure with its own characteristic fractal dimension, $D \simeq 1.8$, 2.6, 1.4 and 1.9, respectively. Fuels with a sooting tendency less than about 10 in TSI only experience the first growth stage.

We believe the results presented in this paper are significant for two reasons. First our soot aerosols have evolved from cluster dilute to clusters dense and thereby demonstrate a crossover from diffusion limited cluster aggregation kinetics to percolation. With the crossover in growth mode, comes a crossover in structure as well, and the concept of a superaggregate. The soot aerosol is just one of many solid particulate sols hence these crossovers should occur in any system, aerosol or colloid, given the proper conditions.

Second, these results have significant bearing on models of soot growth and the effects of soot on the environment. Smoke, soot released to the environment, is usually emitted from flames of fuels with high sooting tendency. The smoke released from laminar diffusion flames has the complex, four stage morphology summarized in Table 1. This complex morphology must be reckoned with to understand soot transport, optical, and chemi- and physi-absorptive properties. Future work must determine the extent to which these stages appear in other important flames such as turbulent diffusion flames.

Acknowledgements

This work was supported by NSF Grant CTS0080017 and NASA Grant NAG3-2360.

References

Cai, J., Lu, N., & Sorensen, C. M. (1993). Comparison of size and morphology of soot aggregates as determined by light scattering and electron microscope analysis. *Langmuir*, *9*, 2861–2867.

Calcote, H. F., & Manos, D. M. (1983). Effect of molecular structure on incipient soot formation. *Combustion and Flame*, *49*, 289–304.

Carpineti, M., Ferri, F., & Giglio, M. (1990). Salt-induced fast aggregation of polystyrene latex. *Physical Review A*, *42*, 7347–7354.

D'Anna, A., D'Alesso, A., & Minutolo, P. (1994). In H. Bockhorn (Ed.), *Soot formation in combustion: Mechanisms and models* (p. 83). Heidelberg: Springer.

Dobbins, R. A., Fletcher, R. A., & Chang, H.-C. (1998). The evolution of soot precursor particles in a diffusion flame. *Combustion and Flame*, *115*, 285–298.

Dobbins, R. A., & Megaridis, C. M. (1987). Morphology of flame-generated soot as determined by thermophoretic sampling. *Langmuir*, *3*, 254–259.

Dobbins, R. A., & Subramaniasivam, H. (1994). Soot precursor particles in flames. in: H. Brockhorn (Ed.), *Soot formation in combustion: Mechanism and models* (pp. 290–301). Berlin, Heidelberg: Springer.

Ferri, F. (1997). Use of a charge coupled device camera for low-angle elastic light scattering. *Review of Scientific Instruments*, *68*, 2265–2274.

Frenklach, M. (2002). Reaction mechanism of soot formation in flames. *Physical Chemistry Chemical Physics*, *4*, 2028–2037.

Fry, D., Chakrabarti, A., Kim, W., & Sorensen, C. M. (2004). Structural crossover in dense irreversibly aggregating particulate systems. *Physical Review E*, *69*, 0614011-1–061401-10.

Fry, D., Sintes, T., Chakrabarti, A., & Sorensen, C. M. (2002). Enhanced kinetics and free-volume universality in dense aggregating systems. *Physical Review Letters*, *89*, 148301–148301-4.

Glassman, I. (1988). Soot formation in combustion processes. *Twenty-second symposium (international) on combustion* (pp. 295–311). The Combustion Institute.

Jullien, R., Thouy, R., & Ehrburger-Dolle, F. (1994). Numerical investigation of two-dimensional projections of random fractal aggregates. *Physical Review E*, *50*, 3878–3882.

Jung, S. J., Amal, R., & Raper, J. A. (1996). Monitoring effects of shearing on floc structure using small-angle light scattering. *Powder Technology, 88*, 51–54.

Kim, W., Sorensen, C. M., & Chakrabarti, A. (2004). Universal occurrence of soot superaggregates with a fractal dimension of 2.6 in heavily sooting laminar diffusion flames. *Langmuir, 20*, 3969–3973.

Koylu, U. O., & Faeth, G. M. (1992). Structure of overfire soot in buoyant turbulent diffusion flames at long residence times. *Combustion and Flame, 89*, 140–156.

Lahaye, J., & Prado, G. (1981). Morphology and internal structure of soot and carbon blacks. In: D.C. Siegla, & G.W. Smith (Eds.), *Particulate carbon* (pp. 33–51). New York: Plenum Press.

Martin, J. E., Wilcoxon, J. P., Schaefer, D., & Odinek, J. (1990). Fast aggregation of colloidal silica. *Physical Review A, 41*, 4379–4391.

Meakin, P. (1999). A historical introduction to computer models for fractal aggregates. *Journal of Sol–Gel Science and Technology, 15*, 97–117.

Oh, C., & Sorensen, C. M. (1997). Light scattering study of fractal cluster aggregation near the free molecular regime. *Journal of Aerosol Science, 28*, 937–957.

Olson, D. B., Pickens, J. C., & Gill, R. J. (1985). The effects of molecular structure on soot formation II. Diffusion flames. *Combustion and Flame, 62*, 43–60.

Palmer, H. B., & Cullis, H. F. (1965). *The chemistry and physics of carbon* (vol. 1, 205). New York: Marcel Dekker.

Samson, R. J., Mulholland, G. W., & Gentry, J. W. (1987). Structural analysis of soot agglomerates. *Langmuir, 3*, 272–281.

Selomulya, C., Bushell, G., Amal, R., & Waite, T. D. (2002). Aggregation mechanisms of latex of different particle sizes in a controlled shear environment. *Langmuir, 18*, 1974–1984.

Sorensen, C. M. (2001). Light scattering by fractal aggregates: A review. *Aerosol Science and Technology, 35*, 648–687.

Sorensen, C. M., Cai, J., & Lu, N. (1992). Light-scattering measurements of monomer size, monomers per aggregate, and fractal dimension for soot aggregates in flames. *Applied Optics, 31*, 6547–6557.

Sorensen, C. M., & Hageman, W. B. (2001). Two-dimensional soot. *Langmuir, 17*, 5431–5434.

Sorensen, C. M., Hageman, W. B., Rush, T. J., Huang, H., & Oh, C. (1998). Aerogelation in a flame soot aerosol. *Physical Review Letters, 80*, 1782–1785.

Sorensen, C. M., Kim, W., Fry, D., Shi, D., & Chakrabarti, A. (2003). Observation of soot superaggregates with a fractal dimension of 2.6 in laminar acetylene/air diffusion flames. *Langmuir, 19*, 7560–7563.

Stauffer, D., & Aharony, A. (1992). *Introduction to percolation theory*. London: Taylor and Francis.

Zhang, H. X., Sorensen, C. M., Ramer, E. R., Olivier, B. J., & Merklin, J. F. (1988). In situ optical structure factor measurements of an aggregating soot aerosol. *Langmuir, 4*, 867–871.